Solvent-Mediated Electronic Coupling: The Role of Solvent Placement

I. Read,[†] A. Napper,[†] R. Kaplan,[‡] M. B. Zimmt,*[,‡] and D. H. Waldeck*[,†]

Contribution from the Departments of Chemistry, University of Pittsburgh, Pittsburgh, Pennsylvania 15260, and Brown University, Providence, Rhode Island 02912

Received July 1, 1999. Revised Manuscript Received September 15, 1999

Abstract: The role of solvent location in mediating electronic coupling between electron donor and acceptor groups is investigated. The temperature-dependent electron-transfer rate constant in a C-clamp shaped donor−bridge−acceptor (DBA) molecule with a 7-Å donor-to-acceptor separation is used to evaluate the solvent reorganization energy and the electronic interaction between the donor and acceptor sites. By studying the reaction in an homologous series of alkylbenzene solvents, it is demonstrated that the donor−acceptor electronic interaction is greatly reduced in solvents that are too bulky for their aromatic ring to position itself between the donor and acceptor groups. The temperature dependence of the reaction free energy for charge separation, $\Delta_r G$, is directly determined from the experimental data. This allows parametrization of a molecular-based solvation model and provides a means to estimate the outer-sphere reorganization energy and its temperature dependence in aromatic solvents.

I. Introduction

Electronic coupling between donor and acceptor sites is a prerequisite for electron-transfer reactions. Covalent bond "mediation" of this coupling is very important for intramolecular electron-transfer reactions, although alternate coupling pathways have been proposed. For example, hydrogen bonds and van der Waals contacts are believed to be important in mediating the electronic coupling for electron-transfer reactions in biomolecules.[1] Recent studies[2−4] have exploited the dependence of bond-mediated coupling magnitudes on the topology of donor−bridge−acceptor (D−B−A) molecules to quantify the relative importance of coupling pathways involving solvent molecules. Although the latter pathways are usually less important than bond-mediated coupling pathways for electron transfer across linear spacers, pathways involving solvents are expected to be important in intermolecular electron-transfer reactions and for intramolecular electron-transfer reactions involving highly curved spacers.

By studying the kinetics of electron transfer across highly curved donor−bridge−acceptor molecules in strongly polar solvents, it has been possible to demonstrate the participation of solvent in mediating the D−A electronic interaction, a phenomenon referred to as "solvent-mediated superexchange".[2,3] Detailed analyses of the temperature dependence of the electron-transfer rate constants were used to extract the electronic coupling matrix element, $|V|$, as a function of spacer topology and solvent. These analyses demonstrated a significant enhancement of D−A coupling for the "C-clamp" system **2** in the aromatic solvent benzonitrile, whereas no solvent dependence was found for the "linear" D−B−A molecule **1** (Chart 1). Additional evidence for solvent-mediated superexchange in electron transfer across U-shaped intramolecular systems was found by Paddon-Row and co-workers.[4] Solvent-mediated superexchange coupling in intermolecular electron-transfer reactions has also been identified in fluid solutions by Gould and Farid[5] and in frozen glasses by Miller.[6]

A deficiency in the earlier studies of **2** is the absence of experimental information that identifies the spatial placement of the solvent molecules most effective at mediating the electronic coupling. Prior theoretical studies indicated that the solvent molecule must lie within the cleft of **2** to produce significant coupling.[7] Unfortunately, experimental efforts to prove the presence and importance of solvent within the cleft were not successful. As an alternative, this study compares the electronic coupling in solvents that can position an aromatic ring within the cleft interior with those that cannot. To this end, electron-transfer rate constants have been determined for **2** in a series of increasingly bulky alkylbenzene solvents (Chart 2). Consideration of van der Waals radii and molecular mechanics calculations indicate that benzene and the monoalkylated benzenes can access geometries in which their aromatic core achieves overlap with both the donor and acceptor π-functions of **2**. The steric bulk provided by the isopropyl groups prohibits

[†] University of Pittsburgh.
[‡] Brown University.

(1) Onuchic, J. N.; Beratan, D. N. *J. Chem. Phys.* **1990**, *92*, 722.
(2) (a) Kumar, K.; Lin, Z.; Waldeck, D. H.; Zimmt, M. B. *J. Am. Chem. Soc.* **1996**, *118*, 243. (b) Han, H.; Zimmt, M. B. *J. Am. Chem. Soc.* **1998**, *120*, 8001.
(3) Kumar, K.; Kurnikov, I. V.; Beratan, D. N.; Waldeck, D. H.; Zimmt, M. B. *J. Phys. Chem. A* **1998**, *102*, 5529.
(4) (a) Oevering, H.; Paddon-Row, M. N.; Heppener, M.; Oliver, A. M.; Cotsaris, E.; Verhoeven, J. W.; Hush, N. S. *J. Am. Chem. Soc.* **1987**, *109*, 3258. (b) Oliver, A. M.; Craig, D. C.; Paddon-Row, M. N.; Kroon, J.; Verhoeven, J. W. *Chem. Phys. Lett.* **1988**, *150*, 366. (c) Warman, J. M.; Smit, K. J.; de Haas, M. P.; Jonker, S. A.; Paddon-Row, M. N.; Oliver, A. M.; Kroon, J.; Oevering, H.; Verhoeven, J. W. *J. Phys. Chem.* **1991**, *95*, 1979. (d) Lawson, J. M.; Paddon-Row, M. N.; Schuddeboom, W.; Warman, J. M.; Clayton, A. H. A.; Ghiggino, K. P. *J. Phys. Chem.* **1993**, *97*, 13099. (e) Roest, M. R.; Verhoeven, J. W.; Schuddeboom, W.; Warman, J. M.; Lawson, J. M.; Paddon-Row, M. N. *J. Am. Chem. Soc.* **1996**, *118*, 1762. (f) Jolliffe, K. A.; Bell, T. D. M.; Ghiggino, K. P.; Langford, S. J.; Paddon-Row, M. N. *Angew. Chem., Intl. Ed. Engl.* **1998**, *37*, 916.
(5) Gould, I.; Farid, S. *J. Am. Chem. Soc.* **1994**, *116*, 8176.
(6) Miller, J. R.; Beitz, J. V. *J. Chem. Phys.* **1981**, *74*, 6746.
(7) Cave, R. J.; Newton, M. D.; Kumar, K.; Zimmt, M. B. *J. Phys. Chem.* **1995**, *99*, 17501.

10.1021/ja992281k CCC: $18.00
Published on Web 11/10/1999

Chart 1. Chemical Structures of Donor−Bridge−Acceptor Molecules, A7DCE (**1**) and A9DCE (**2**), Are Shown with Their CPK Renderings

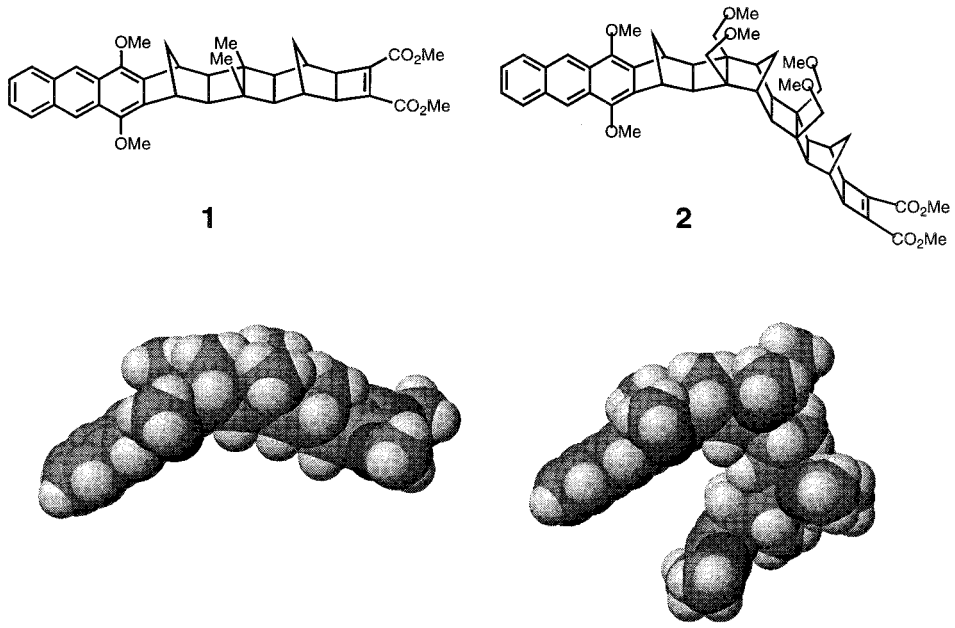

Chart 2. Chemical Structures of the Solvents Used in This Work

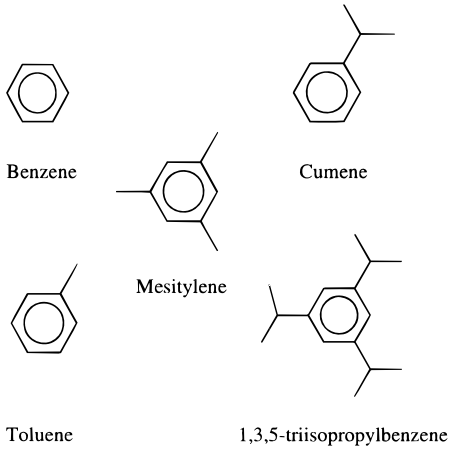

such simultaneous overlap for 1,3,5-triisopropylbenzene (TIP). The lowest energy conformation of the isopropyl group projects a methyl group above and below the ring plane. The thickness of the molecule is increased in the vicinity of the isopropyl group and this affects the placement of the solvent's aromatic core within the cleft of **2**. Chart 3 displays the results of molecular mechanics energy minimizations for **2** with cumene (A) or TIP (B and C). The heavy line connects the 9-position of the anthracene with the acceptor alkene carbon. When the isopropyl group of cumene projects down (Chart 3A), the aromatic ring is simultaneously in close proximity to both the anthracene and the alkene acceptor. With TIP, either one isopropyl group (C) or two isopropyl groups (B) must project into the cleft. Although the cleft appears to widen slightly to accommodate this solvent, its aromatic core is significantly further down in the cleft (Chart 3B,C) and farther from either the D or A group. If solvent-mediated coupling in **2** requires the solvent's aromatic core to be simultaneously proximate to both the D and A group, the experimentally determined coupling magnitude should decrease with increasing steric bulk of the solvent molecules. This effect has been experimentally observed.

Although the fluorescence decays from **2** in polar solvents[2,3] exhibited single exponential kinetics, the kinetics observed in these weakly polar aromatic solvents are not single exponential. Instead, they are well fit using biexponential rate expressions. This feature allows determination of both the forward $k_{for}(T)$ and reverse $k_{back}(T)$ electron-transfer rates and, consequently, the free energy of the charge separation reaction, $\Delta_r G(T)$. Direct knowledge of $\Delta_r G(T)$ restricts the number of adjustable parameters in the semiclassical model (eq 6) and allows robust conclusions to be drawn concerning the solvent dependence of the electronic coupling. In addition, the experimental $\Delta_r G(T)$ data is used to calibrate a molecular-based model for the solvation energy and the reorganization energy λ_o in weakly polar and nonpolar solvents.[8] This sophisticated treatment of the outer-sphere reorganization energy produces values that are in reasonable agreement with those extracted from the rate constant data, $k_{ET}(T)$, assuming temperature independent values of λ_o and the electronic coupling $|V|$.

The paper is organized as follows. Experimental and computational details as well as a general summary of the observations are provided in section II. In section III, the need for temperature-dependent outer-sphere reorganization energy and electronic coupling parameters is evaluated through analysis of the $k_{ET}(T)$ data with the semiclassical model (eq 6) and the experimentally determined $\Delta_r G(T)$. Section IV describes the parametrization of a molecular solvation model using the $\Delta_r G(T)$ data. In section V, the parametrized model is then used to predict the temperature dependence of the outer-sphere reorganization energy and to estimate the electronic coupling. The final section summarizes the findings and draws conclusions.

II. Experimental Section

A. Materials and Equipment. The preparation of compounds **1** and **2** has been reported elsewhere.[9] The compounds were stored in a refrigerated desiccator. The optical density of the samples was ~0.05

(8) (a) Matyushov, D. V. *Chem. Phys.* **1996**, *211*, 47. (b) Matyushov, D. V.; Schmid, R. *Mol. Phys.* **1995**, *84*, 533. (c) Matyushov, D. V.; Schmid, R. *J. Chem. Phys.* **1995**, *103*, 2034.

(9) Kumar, K.; Tepper, R. J.; Zeng, Y.; Zimmt, M. B. *J. Org. Chem.* **1995**, *60*, 4051.

Chart 3. Results of Molecular Mechanics Energy Minimizations for **2** with Cumene (A) or TIP (B, C)[a]

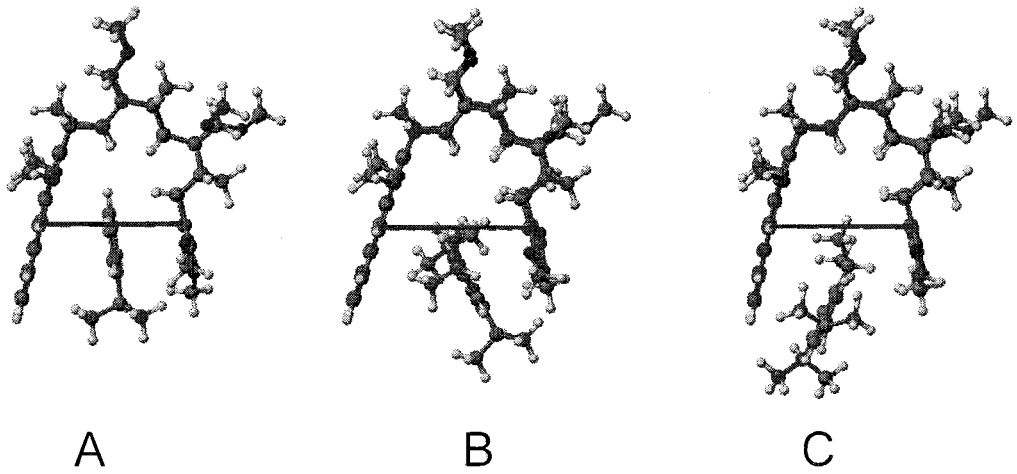

[a] Compound **2** and TIP are displayed as ball and stick renderings. The heavy line connects the anthracene **9** position and the acceptor alkene C.

at the excitation wavelength. All solvents were purified in the following manner. First, the solvent was thoroughly washed with concentrated H_2SO_4 until the acid layer remained colorless upon vigorous shaking. Next, the solvent was washed several times with deionized water and dried over $MgSO_4$. Finally, the solvent was fractionally distilled over sodium. In each case, the solvent was freshly distilled for sample preparation. The samples were then freeze−thaw−degassed three times to prevent oxygen quenching of the long lifetime component of the decay law. At higher temperatures, a positive argon (Matheson Inc., 99.99%) pressure was applied to the sample to prevent evaporation of the solvent from the heated section.

The time-correlated single photon counting method was used to measure the fluorescence intensity decays from the locally excited state of the anthracene. The sample was excited by 375-nm radiation from a frequency-doubled 750-nm dye laser pulse. The dye laser pulse train had a repetition rate of ~300 kHz and was generated by a cavity-dumped and synchronously pumped Coherent CR-599 dye laser. The pulse energies were kept below 1 nJ, and the count rates were kept below 4 kHz. All fluorescence measurements were made at the magic angle. Other particulars of the apparatus have been reported elsewhere.[10] The temperature cell was constructed from aluminum and controlled using a NESLAB RTE-110 chiller. Temperature measurements were taken at the sample using a Type-K thermocouple (Fisher-Scientific) accurate to within 0.5 °C.

The fluorescence decays were fit to a sum of two exponential terms using the Marquardt−Levenberg nonlinear least squares algorithm. In each case the decay law was convolved with the instrument response function, measured by scattering from a $BaSO_4$ colloid, and compared to the observed decay. Fitting to the semiclassical rate equation and the molecular based model calculations of the reorganization energies and reaction free energies were performed using Microsoft Excel 7.0. The FCWDS sum in eq 6 converges rapidly and was not evaluated beyond the sixth term.

B. Kinetic and Thermodynamic Analyses. In prior studies involving polar solvents,[2,3] the time evolution of the anthracene's lowest excited state (LE) fluorescence was adequately described by a single-exponential decay law. This indicated irreversible electron transfer to the acceptor; i.e., generation of the charge transfer state (CT). By contrast, in nonpolar solvents, the decay of the LE state is found to exhibit a double exponential decay law.[11] Figure 1 shows a fluorescence decay for **2** in mesitylene at 50 °C. The best fit parameters are $\tau_1 =$ 0.909 ns (51.7%) and $\tau_2 = 19.3$ ns (48.3%). The anthracene fluorescence data in the alkylated aromatic solvents was analyzed assuming interconversion of the lowest energy singlet excited states, LE and CT (Figure 2).

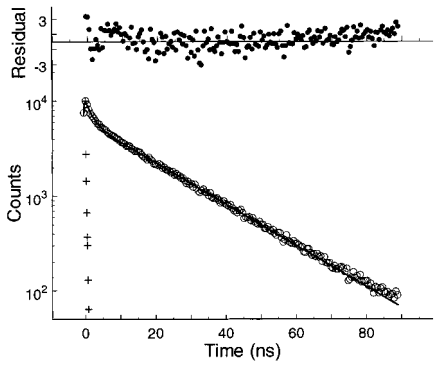

Figure 1. A fluorescence decay profile (circles) is shown for A9DCE in mesitylene at 50° C. The instrument function (+) is also shown. The best fit to a double exponential (line) gives $\tau_1 = 0.909$ ns (51.7%); $\tau_2 = 19.3$ ps (48.3%); and a $\chi^2 = 1.5$. The residuals for the fit are also shown.

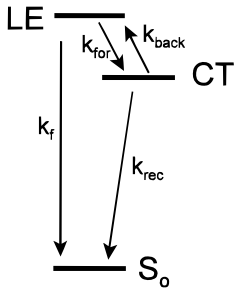

Figure 2. This diagram shows the kinetic scheme used to interpret the fluorescence intensity decay from **2** in the alkylated benzene solvents.

Table 1 displays lifetime parameters determined at selected temperatures in the alkylated benzene solvents. For the aromatic solvents other than TIP, increasing the number or size of the alkyl groups on the benzene core, or increasing the sample temperature, generates an increase in the value of the fast component lifetime and a decrease in the fast component amplitude, A_1. Qualitatively, this suggests that the charge separation rate constant decreases with increasing temperature or with increasing alkyl substitution of the benzene ring. To quantify these variations, the solvent and temperature dependence of the decay parameters were interpreted using the kinetic scheme illustrated in

(10) (a) Zeglinski, D. M.; Waldeck, D. H. *J. Phys. Chem.* **1988**, *92*, 692. (b) O'Connor, D. V.; Phillips, D. *Time Correlated Single Photon Counting*; Academic Press: New York, 1984.

(11) (a) Heitele, H.; Finckh, P.; Weeren, S.; Pöllinger, F.; Michel-Beyerle, M. E. *J. Phys. Chem.* **1989**, *93*, 5173. (b) Kroon, J.; Oevering, H.; Verhoeven, J. W.; Warman, J. M.; Oliver, A. M.; Paddon-Row, M. N. *J. Phys. Chem.* **1993**, *97*, 5065. (c) Asahi, T.; Ohkohchi, M.; Matsusaka, R.; Mataga, N.; Zhang, R. P.; Osuka, A.; Maruyama, K. *J. Am. Chem. Soc.* **1993**, *115*, 5665.

Table 1. Kinetic Parameters for **2** in Different Solvents as a Function of Solvent Polarity[a]

solvent	τ_1, ps (A_1)	T, K	V, Å^3	ϵ_S	n^2
benzene	325 (99%)	296	148	2.27	2.25
benzene	409 (90%)	342	148	2.19	2.18
toluene	371 (97%)	296	176	2.38	2.24
toluene	463 (69%)	347	176	2.26	2.15
cumene	586 (90%)	296	232	2.38	2.22
cumene	746 (47%)	345	232	2.28	2.13
mesitylene	678 (82%)	296	231	2.27	2.25
mesitylene	909 (52%)	323	231	2.27	2.25
TIP	3260 (68%)	260	397	2.29[c]	2.26[d]
TIP[b]	1720 (51%)	283	397	2.27[c]	2.23

[a] The long component time constant is 15−25 ns in each case. [b] TIP is 1,3,5-triisopropylbenzene. [c] The static dielectric constant for triisopropylbenzene could not be found in the literature. The value given here is that of triethylbenzene. [d] Experimentally determined.

Figure 2, where k_{for} is the forward (charge separation) electron-transfer rate constant (LE → CT), k_{back} is the reverse electron-transfer rate constant (CT → LE), k_{rec} is the sum of the rate constants for irreversible recombination to lower energy electronic states (CT → S_0, T_1) and k_f is the observed decay rate of the LE state in the absence of an electron acceptor. With the reasonable assumption that light excitation populates only the locally excited state and that only emission from this state is observed, one obtains a double exponential decay law for the fluorescence $I(t)$ given by

$$I(t) = a_+ \exp(-k_+ t) + (1 - a_+) \exp(-k_- t) \quad (1)$$

where a_+ is the fraction of the fluorescence decaying with the fast rate constant k_+ and where k_- is the rate constant of the slow fluorescence decay. These parameters are related to the fundamental molecular rate constants by the following relations:

$$k_{for} = a_+(k_+ - k_-) + k_- - k_f \quad (2)$$

$$k_{back} = \frac{(k_+ - k_-)^2 - [2(k_{for} + k_f) - (k_+ + k_-)]^2}{4k_{for}} \quad (3)$$

and

$$k_{rec} = k_+ + k_- - k_f - k_{for} - k_{back} \quad (4)$$

The value of k_f is obtained from measurements of the donor−bridge compound and is very close to 5×10^7 s^{-1} in all the solvents at every temperature. The value of k_- (see footnote *a* to Table 1) was found to vary by as much as 50%, depending on the concentration of trace impurities in the solution. Fortunately, the values of k_{for} and k_{back} depend only weakly on the slow rate constant (as it is much smaller than k_+). The scatter in k_- does generate considerable uncertainty in k_{rec}, however. For this reason only the rate constants k_{for} and k_{back} are compared with the electron-transfer rate theory.

The temperature dependence of the rate constants for the forward (filled symbols) and backward (open symbols) excited-state electron-transfer reactions are plotted in Figure 3. Figure 3A displays the data for the methyl-substituted benzenes, and Figure 3B displays the data for the isopropyl-substituted benzenes. The lines drawn in the graph represent fits to the semiclassical electron-transfer rate equation (vide infra). In the unsubstituted and singly substituted benzene solvents, the charge separation rate constants, k_{for}, exhibit an apparent negative activation energy, whereas the excited-state charge recombination rate constants, k_{back}, exhibit an apparent positive activation energy. In the trisubstituted solvents, the temperature dependence of k_{for} and k_{back} are more complex. In mesitylene, the slope d(ln k_{for})/dT becomes increasingly negative with increasing temperature. At low temperatures, k_{back} increases with increasing temperature, but at higher temperatures, k_{back} becomes temperature independent. In triisopropylbenzene, both k_{for} and k_{back} increase with temperature. This observation of apparent positive activation energies for both the charge separation and recombination steps is unique among the five aromatic solvents investigated. The amount of scatter in the TIP data is greater than in the other solvents because the two rate constants for the fluorescence decay are more similar in magnitude, making it more difficult to extract the rate constants reliably. The two decay components are similar because the values of k_{for} and k_{back} are smaller in TIP as compared to the other solvents (Table 1). Nonmonotonic and "negative" temperature dependence of electron-transfer rate constants of DBA systems in nonpolar and weakly polar solvents have been reported by other workers.[11] These observations may be explained, in part, by consideration of the temperature dependence of the LE → CT free energy difference.

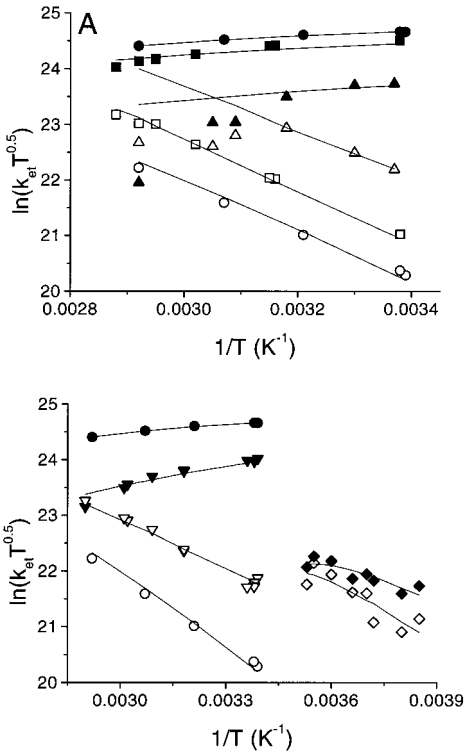

Figure 3. The temperature dependence of the forward (filled symbols) and backward (open symbol) electron-transfer rate constants are shown. Panel A shows the data for benzene (●, ○), toluene (■, □), and mesitylene (▲, △). Panel B shows the data for benzene (●, ○), cumene (▼, ▽), and triisopropylbenzene (♦, ◊). The lines are fits to the data using the Matyushov model for $\Delta_r G(T)$ and d$\lambda_o(T)$/dT.

The value of $\Delta_r G$ (LE → CT) at each temperature was computed from the ratio k_{for}/k_{back} (Figure 4). In each solvent, $\Delta_r G$ increases with increasing temperature; i.e., the charge transfer state is destabilized upon increasing the temperature. The entropy change upon charge separation, $\Delta_r S$, is quite negative, e.g. −22 and −26 cal/(mol K) in benzene and in cumene, respectively. Continuum models (Born, Onsager)[12] and molecular models of solvation[8] both predict the negative sign of $\Delta_r S$. However, simple continuum models predict that $\Delta_r G$ in benzene should be more positive than in either toluene or cumene, in contrast to the experimental results. This contradiction is one of numerous examples[13] that highlight the inability of simple continuum models to predict or rationalize solvation in nonpolar solvents. In an effort to view these results within the framework of a reasonable theory, a molecular model for solvation, developed by Matyushov[8] for dipolar, polarizable, hard-sphere solvents, is employed. As will be described in section IV, this theory reproduces the solvent and temperature variations of $\Delta_r G$ and provides some guidance as to the temperature dependence of the outer-sphere reorganization energy.

(12) (a) Marcus, R. A. *Annu. Rev. Phys. Chem.* **1964**, 15, 155. (b) Marcus, R. A. *J. Chem. Phys.* **1965**, *43*, 679.

(13) (a) Reynolds, L.; Gardecki, J. A.; Frankland, S. J. V.; Horng, M. L.; Maroncelli, M. *J. Phys. Chem.* **1996**, *100*, 10337. (b) Gardecki, J.; Horng, M. L.; Papazyan, A.; Maroncelli, M. *J. Mol. Liq.* **1995**, *65*, 49.

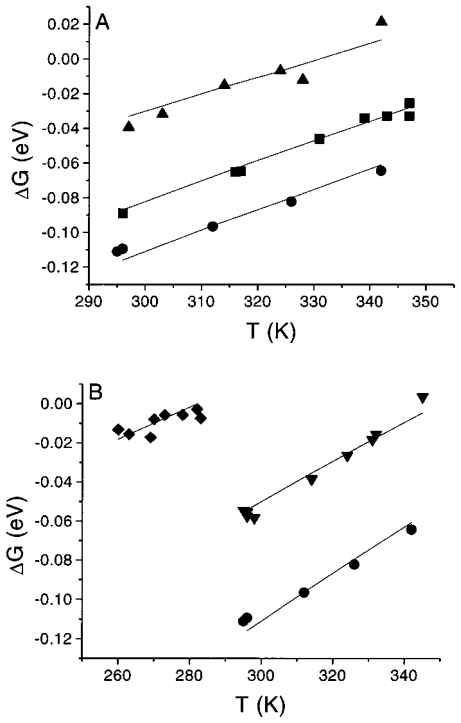

Figure 4. The temperature dependence of $\Delta_r G$ for the electron-transfer reaction is shown. Panel A shows the data for benzene (●), toluene (■), and mesitylene (▲). Panel B shows the data for benzene (●), cumene (▼), and triisopropylbenzene (♦).

III. Analyses

A. Kinetic Models. The donor−acceptor electronic coupling for **2** in the aromatic solvents is much smaller than kT and lies in the nonadiabatic, or weak, coupling regime.[14] In this case, the electron-transfer rate constant may be expressed in terms of the Golden Rule formula:

$$k_{ET} = \frac{2\pi}{\hbar}|V|^2 \mathrm{FCWDS} \tag{5}$$

where $|V|$ is the magnitude of the electronic coupling between the donor and acceptor groups and FCWDS is the Franck−Condon Weighted Density of States. The FCWDS factor accounts for the impact of nuclear coordinates on the electron-transfer rate. As discussed for this DBA system[3] and related ones,[2,4] a semiclassical expression with a single quantized mode provides an adequate description of the rate constant. In particular,

$$k_{ET} = \frac{2\pi|V|^2}{\hbar\sqrt{4\lambda_o \pi k_B T}} \sum_{n=0}^{\infty} e^{-S}\left(\frac{S^n}{n!}\right) \exp\left[\frac{-(\Delta_r G + \lambda_o + nh\nu)^2}{4\lambda_o k_B T}\right] \tag{6}$$

where k_B is Boltzmann's constant, λ_o is the outer-sphere (or solvent) reorganization energy, ν is the frequency of the effective quantized vibrational mode, $\Delta_r G$ is the reaction free energy, and S is the Huang−Rhys factor defined by

$$S = \frac{\lambda_v}{h\nu} \tag{7}$$

in which λ_v is the inner-sphere reorganization energy. The total reorganization energy $\lambda = \lambda_v + \lambda_o$ represents the change in energy if the reactant were to change to the equilibrium configuration of the product without transferring an electron. This model for the rate constant has been widely successful in describing intramolecular electron-transfer processes.[15,16]

The rate expression in eq 6 has five parameters: $\Delta_r G$, λ_v, λ_o, ν, and $|V|$. As noted above, the value of $\Delta_r G$ at each temperature can be obtained directly from the data. The inner-sphere reorganization energy λ_v and the characteristic vibrational frequency ν were previously determined by fitting charge-transfer spectra for a related system (same donor and acceptor units but a shorter bridge unit) and by quantum chemical calculations.[3] Those studies found that $\lambda_v = 0.39$ eV and $h\nu = 0.175$ eV were reasonable parameter values. These two quantities reflect the changes in the nuclear arrangement of the anthracene upon oxidation and of the acceptor upon reduction. As such, one expects the two parameters to remain nearly constant with changes in the bridge that are remote from the D or A group, or with changes in the solvent.[3] One potential caveat is raised by the recent computational work of Paddon-Row[17] which suggests that the D−A separation (in vacuo) changes significantly in the Coulomb field of the charge separated state. For **2**, such distortions could result in different $|\Delta_r G|$, λ_v, λ_o, and $|V|$ for the forward and back electron-transfer steps. We have found no particular evidence supporting this behavior in these solvents. Thus, two parameters, $|V|$ and λ_o, remain to be determined from the electron-transfer rate constants and their temperature dependence.

Considerable "parameter coupling" arises between the best fit values of the fitting parameters when analyzing temperature-dependent data. This issue has been discussed at length for these DBA systems in other solvents.[3] The availability of the "correct" value of $\Delta_r G$ from the ratio of k_{for}/k_{back} at each temperature greatly simplifies the task of extracting accurate values of λ_o and $|V|$. Nevertheless, a parametric relationship exists between the remaining two parameters, λ_o and $|V|$, at each temperature. This relationship is exhibited in Figure 5 for benzene, cumene, and triisopropylbenzene at selected temperatures. This figure shows that the value of $|V|$ that is required to reproduce k_{for} varies nonlinearly with the assumed value of the outer-sphere reorganization energy. For these solvents, the parametric relationship varies only slightly with temperature (vide infra). The curves in Figure 5 support two limiting conclusions: (1) if λ_o is relatively constant in all three solvents, $|V|$ in benzene and cumene are nearly equal but $|V|$ in TIP is at least three times smaller or (2) if $|V|$ in TIP is the same magnitude as $|V|$ in benzene, λ_o must be ~0.1 eV (30−50%) larger in TIP than in benzene. Some combination of these explanations is also possible.

If one makes the conventional assumption that the electronic coupling $|V|$ is temperature independent, it is possible to determine the temperature dependence of the outer-sphere reorganization energy from k_{for}.[18] However, it is possible that *solvent*-mediated electronic coupling (in contrast to *bond*-mediated electronic coupling) is temperature-dependent. Consequently, the analysis of the k_{ET} data proceeds in stages. First, the rate constant data are analyzed with the assumption that $|V|$ is temperature-independent. This allows the apparent temper-

(14) Jortner, J. *J. Chem. Phys*. **1976**, *64*, 4860.

(15) (a) Meyer, T. J. *Prog. Inorg. Chem.* **1983**, *30*, 389. (b) Miller, J. R.; Beitz, J. V.; Huddleston, R. K. *J. Am. Chem. Soc.* **1984**, *106*, 5057.

(16) Barbara, P. F.; Meyer, T. J.; Ratner, M. A. *J. Phys. Chem.* **1996**, *100*, 13148.

(17) Shephard, M. H.; Paddon-Row, M. N. *J. Phys. Chem. A* **1999**, *103*, 3347.

(18) (a) Hupp, J. T.; Neyhard, G. A.; Meyer, T. J. *J. Phys. Chem.* **1992**, *96*, 10820. (b) Dong, Y.; Hupp, J. T. *Inorg. Chem*. **1992**, *31*, 3322. (c) Dong, Y.; Hupp, J. T. *J. Am. Chem. Soc.* **1993**, *115*, 6428.

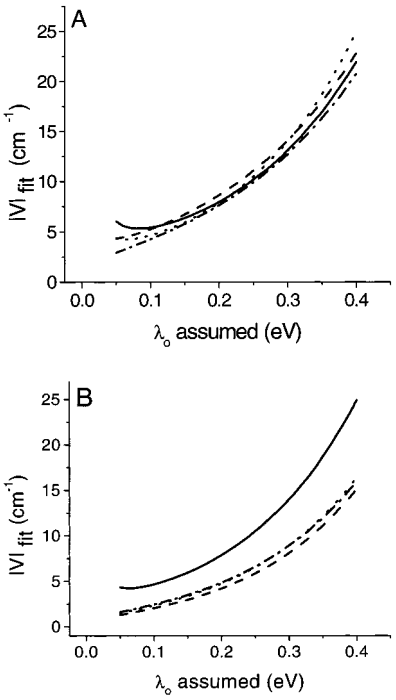

Figure 5. This figure illustrates the parameter coupling between $|V|$ and λ_o. Panel A shows the data for benzene (295 K, solid line), benzene (342 K, dashed line), cumene (270 K, dotted line), cumene (345 K, dash−dot line). Panel B shows the data for cumene (270 K, solid line), triisopropylbenzene (260 K, dashed line), triisopropylbenzene (270 K, dotted line), triisopropylbenzene (283 K, dash−dot line). The 270 and 283 K curves overlap in panel B.

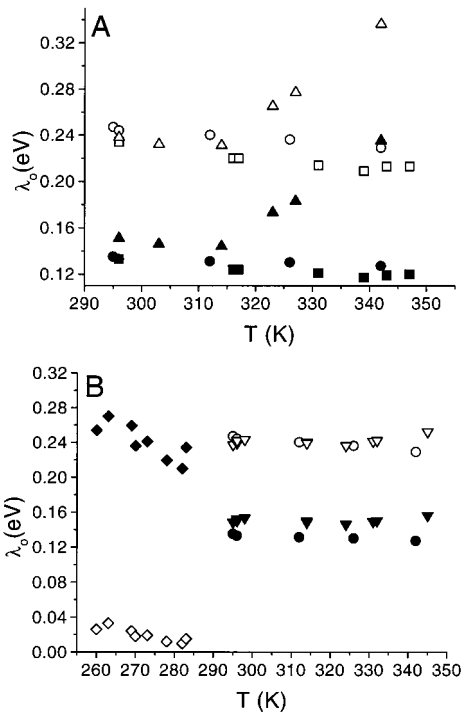

Figure 6. The temperature-dependent values of λ_o that are needed to reproduce the $k_{for}(T)$. Panel A shows the data for benzene (●, ○), toluene (■, □), and mesitylene (▲, △). Panel B shows the data for benzene (●, ○), cumene (▼, ▽), and triisopropylbenzene (♦, ◊). The filled symbols give values of λ_o for $|V| = 6$ cm^{-1}. The open symbols give values of λ_o for $|V| = 10$ cm^{-1} for all the solvents except TIP where it was set to $|V| = 1$ cm^{-1}.

ature dependence of the reorganization energy to be extracted from $k_{for}(T)$. For the solvents in which λ_o changes little over a reasonable range of temperatures, the rate constant data can be fit to eq 6 with $|V|$ and λ_o as temperature-independent fitting parameters. Next, a molecular model for solvation is parametrized using the $\Delta_r G(T)$ data. This model is used to predict the temperature dependence of the solvent reorganization energy. The kinetic data are then analyzed using the parametrized model in two ways. Initially, the model is used to predict the $\Delta_r G(T)$ and $d\lambda_o/dT$ values so that $|V|$ and $\lambda_o(295)$ are the adjustable fitting parameters. Finally, the model is more stringently tested by using the predicted $\Delta_r G(T)$ and $\lambda_o(T)$ values with $|V|$ as the only adjustable fitting parameter.

B. Is λ_o Temperature-Dependent? With values of 0.39 eV for λ_v, 0.175 eV for $h\nu$ and $\Delta_r G(T)$ available from the data, it is possible to obtain $\lambda_o(T)$ if a value for the electronic coupling $|V|$ can be found. As one goal of this study is to learn more about the temperature dependence of λ_o, we proceed by assuming a reasonable value for $|V|$ and then extract $\lambda_o(T)$ from the data using eq 6. Figure 6 displays the outer-sphere reorganization energies $\lambda_o(T)$ required to reproduce the $k_{for}(T)$ data for two different assumed values of the electronic coupling in the different methylbenzene (panel A) and isopropylbenzene (panel B) solvents. As was evident in Figure 5, larger values of $|V|$ produce larger values of λ_o. For both assumed values of $|V|$, the required $\lambda_o(T)$ values in benzene decrease very slightly with temperature. The required $\lambda_o(T)$ values in toluene exhibit a similar magnitude and temperature dependence as the benzene values for the same assumed $|V|$. This result is consistent with the similar electron-transfer rate constants in benzene and toluene, and these solvents' similar properties. Below 320 K, the required λ_o in mesitylene is within 0.02 eV of that in benzene, for the same $|V|$. However, above 320 K, the λ_o generated by this analysis rises steeply. In clear contrast to benzene and toluene, some property of mesitylene varies strongly with temperature. Comparing the open symbols ($|V| = 10$ cm^{-1}) and the solid symbols ($|V| = 6$ cm^{-1}), the absolute value of the reorganization energy is rescaled, but its temperature dependence is not affected. Panel B shows that the required values of λ_o in cumene are also within 0.02 eV of those for benzene and, as seen in Figure 5, appear to increase slightly above 330 K. For the case of $|V| = 6$ cm^{-1}, the required λ_o in TIP is almost double that of benzene and exhibits a steep, negative temperature dependence. Use of a smaller $|V|$ for TIP (open symbols, $|V| = 1$ cm^{-1}) produces smaller values of λ_o and a weaker temperature dependence.

The foregoing analyses indicate that it is reasonable to treat $|V|$ and λ_o as temperature-independent in benzene, toluene, and cumene. Upon close inspection, either λ_o decreases slightly or $|V|$ increases slightly with increasing temperature in benzene and toluene. A similar situation appears to exist for mesitylene below 320 K. By contrast, it is not reasonable to treat $|V|$ and λ_o as temperature-independent in triisopropylbenzene unless the absolute magnitude of $|V|$ is significantly smaller than 6 cm^{-1}. If $|V|$ is 6 cm^{-1} or greater in TIP, then λ_o must decrease with increasing temperature or $|V|$ must be temperature-dependent. The opposite situation appears to hold in mesitylene above 320 K; either $|V|$ decreases or λ_o increases sharply with increasing temperature. To determine the magnitude and possible temperature dependence of $|V|$ requires a reasonable model for the magnitude and/or temperature dependence of λ_o in these solvents. Continuum models are not able to predict the temperature dependence, let alone the magnitude, of λ_o in these aromatic solvents. To estimate the magnitude and temperature dependence of λ_o, a molecular-based model for the solvation energy and solvent reorganization energy was explored. The

analysis and resulting estimates of $|V|$ and λ_o are described in the next section.

IV. Modeling $\Delta_r G(T)$ and $\lambda_o(T)$

Modeling $\Delta_r G(T)$ and $\lambda_o(T)$ in the alkylbenzenes is expected to be nontrivial because of their nondipolar character. Hence one expects the dispersion and induction forces to play a significant role in the solvation and its temperature dependence.[8] In addition, the importance of quadrupole and higher order moments should, in principle, be considered. Although theoretical efforts to include such contributions are under development, their implementation remains difficult and their reliability has not been assessed.[19] The description of the solvent dependence of $\Delta_r G(T)$ and $\lambda_o(T)$ used here employs a reference hard-sphere, dipolar polarizable fluid to account for the effects of solvent density variation on the solvation and hence its temperature dependence. The model accounts for both induction and dispersion forces.[8]

Matyushov[8] writes the reaction free energy $\Delta_r G$ as a sum of three components:

$$\Delta_r G = \Delta G_{\text{vacuum}} + \Delta G_{\text{dipole}} + \Delta G_{\text{dispersion}} \tag{8}$$

where ΔG_{vacuum} is the reaction free energy in a vacuum. The ΔG_{dipole} term contains contributions from the dipole−dipole interaction between the solute and solvent and the induction force between the solute dipole and the solvent. This term is given by[20]

$$\Delta G_{\text{dipole}} = -\frac{\Delta m}{\sigma^3}(m_e' + m_g')P(y,\rho^*,r_0) \tag{9}$$

where σ is the hard-sphere diameter of the solvent, ρ^* is the reduced solvent density $\rho\sigma^3$ (ρ is the solvent number density), r_0 is the distance of closest approach between the solute and solvent in reduced units ($r_0 \equiv 0.5 + R_0/\sigma$ where R_0 is the effective radius of the solute molecule—approximated as a sphere), and y is the solvent's zero frequency dipolar density ($y = (4\pi/9kT)\rho m_s^2 + (4\pi/3)\rho\alpha_s$) arising from solvent permanent dipole moments m_s and solvent molecule polarizability α_s. The difference in dipole moment between the solute CT state, m_e, and LE state, m_g, is given by Δm. The solute dipole moments are renormalized as a consequence of the solute polarizability. The slanted prime indicates a renormalized magnitude induced by the solvent's zero frequency dipolar density, y:

$$m' = \frac{m}{\left[1 - \dfrac{2\alpha_0 P(y,\rho^*,r_0)}{\sigma^3}\right]} \tag{10}$$

where α_0 is the solute polarizability. The functions $P(y,\rho^*,r_0)$ are Pade approximants to the dipolar response function of the fluid. Their explicit form is given in Appendix A.

The third term $\Delta G_{\text{dispersion}}$ is the contribution to the free energy from the dispersion interactions between the solute and solvent. It is given by

$$\Delta G_{\text{dispersion}} = \frac{\Delta\gamma'}{\alpha_s} 96\eta\epsilon_{LJ}^s\left(\frac{\sigma}{\sigma^{0s}}\right)^6 \int_{\sigma_{LJ}^{0s}}^{\infty} u_1^{0s}(r)\, g_{0s}^{(0)}(r) r^2\, dr \tag{11}$$

where η is the solvent-packing fraction of the hard-sphere solvent, $\sigma^{0s} = R_0 + \sigma/2$ is the effective solvent−solute diameter, ϵ_{LJ}^s is the solvent Lennard-Jones energy and $g_{0s}^{(0)}$ is the solute−solvent hard-sphere distribution function. The hard-sphere diameter σ was used for the Lennard-Jones diameter of the solvent in the Matyushov formulation. The term $u_1^{0s}(r)$ is equal to $u^{0s}(r)\theta(r - \sigma^{0s})$ where $u^{0s}(r)$ is the Lennard-Jones potential function and $\theta(x)$ is the Heaviside function. The term $\Delta\gamma'$ is the change in solute polarizability between the LE and CT states weighted by a ratio of solute and solvent ionization potentials.[8] Here it was treated as an adjustable solute parameter. These expressions may be evaluated, given the appropriate solute and solvent parameters, and compared to the experimentally determined free energy changes.

Matyushov[8] also derived an expression for λ_o, the outer-sphere reorganization energy upon electron transfer, which has three sources:

$$\lambda_o = \lambda_{\text{dipole}} + \lambda_{\text{dispersion}} + \lambda_{\text{induction}} \tag{12}$$

The dipolar contribution λ_{dipole} is given by

$$\lambda_{\text{dipole}} = \frac{\Delta m}{\sigma^3}[(m_e' - m_g')P(y,\rho^*,r_0) - (m_e^{\infty} - m_g^{\infty})P(y_{\infty},\rho^*,r_0)] \tag{13}$$

The m^{∞} terms reflect solute dipole renormalization by the high-frequency dipolar density that arises from the solvent polarizability. The dispersion contribution to the reorganization energy $\lambda_{\text{dispersion}}$ is given by[20]

$$\lambda_{\text{dispersion}} = \frac{8\eta}{3}\beta(\epsilon_{LJ}^s\Delta\gamma')^2[\int_0^{\infty} u_1^{0s}(r)^2 g_{0s}^{(0)}(r) r^2\, dr - (1 - m_{ss}(0))\int_0^{\infty} u_1^{0s}(r) u_1^{0s}(r + \phi) g_{0s}^{(0)}(r) g_{0s}^{(0)}(r + \phi) r(r + \phi)\, dr] \tag{14}$$

where $m_{ss}(0) = (1 - \eta)^4/(1 + 2\eta)^2$ and the phase factor ϕ is given as a function of η in Appendix A. The induction contribution $\lambda_{\text{induction}}$ is given by

$$\lambda_{\text{induction}} = \frac{1}{\eta k_B T}\left(\frac{\Delta m'^2 y_{\infty}}{20\sigma^3}\right)^2 [4(2m_{\infty}^{+}(0) + m_{\infty}^{-}(0)) - 9] \times 9\int_{r_0}^{\infty} \frac{g_{0s}^{(0)}(r)}{r^{10}} dr \tag{15}$$

where

$$m_{\infty}^{+}(0) = \frac{1}{3y_{\infty}}\left(1 - \frac{1}{\epsilon_{\infty}}\right) \tag{16a}$$

and

$$m_{\infty}^{-}(0) = \frac{1}{3y_{\infty}}(\epsilon_{\infty} - 1) \tag{16b}$$

As with the free-energy expressions, this sum must be evaluated for an appropriate choice of solute and solvent parameters.

Equations 8−11 were used to reproduce the experimental values of $\Delta_r G$ and its temperature dependence. Unknown

(19) (a) Chitanvis, S. M. *J. Chem. Phys.* **1996**, *104*, 9065. (b) Koga, K.; Tanaka, H.; Zeng, X. C. *J. Phys. Chem.* **1996**, *100*, 16711. (c) Bliznyuk, A. A.; Gready, J. E. *J. Phys. Chem.* **1995**, *99*, 14506. (d) Kim, H. J. *J. Chem. Phys.* **1996**, *105*, 6818. (e) Perng, B.-C.; Newton, M. D.; Raineri, F. O.; Friedman, H. L. *J. Chem. Phys.* **1996**, *104*, 713. (f) Perng, B.-C.; Newton, M. D.; Raineri, F. O.; Friedman, H. L. *J. Chem. Phys.* **1996**, *104*, 7177.

(20) Equations 9 and 14 given here are a correction of the originally published equations (ref 8). The authors thank Dmitry Matyushov for pointing out the errors.

Table 2. Solvent Parameters Used in the Matyushov Modeling

solvent	m, D[a]	σ, Å[b]	α_0, Å^3 [c]	ϵ_{LJ}^s,k_B	η(296)	$d\lambda_o(T)/dT$, eV/K
benzene	0.01	5.277	10.7	544	0.518	-2.2×10^{-4}
toluene	0.31	5.680	11.8	596	0.543	-6.5×10^{-4}
cumene	0.39	6.286	15.5	662	0.560	-7.2×10^{-4}
mesitylene	0.01	6.400	15.3	862	0.593	-4.5×10^{-4}
TIP[d]	0.01	7.400	30.7	1117	0.534	-1.0×10^{-4}

[a] The dipole moments for benzene, mesitylene, and triisopropylbenzene were chosen to be very small but nonzero to facilitate computation. The dipole moments of toluene and cumene were taken from Riddick, J. A.; Bunger, W. B.; Sakano,T.K *Organic Solvents: Physical Properties and Methods of Purification*; Wiley: New York, NY, 1986. [b] The effective hard-sphere diameters and the Lennard-Jones parameters for the solvents were obtained using the method described by Ben-Amotz, D.; Willis, K. G. *J. Phys. Chem.* **1993**, *97*, 7736. [c] The solvent polarizabilities were taken from the CRC. In each case, they were slightly modified to give a good fit. [d] TIP is 1,3,5-triisopropylbenzene.

Table 3. Best Fit Values for $|V|$ and λ_o Using the Experimentally Determined $\Delta_r G(T)$: Method 1

solvent	$\lvert V\rvert$, cm^{-1}	λ_o, eV
benzene	5.6	0.12
toluene	5.1	0.10
cumene	5.0	0.12
mesitylene	3.1	0.050
TIP[a]	1.2	0.023

[a] TIP is 1,3,5-triisopropylbenzene.

Table 4. Best Fit $|V|$ and $\lambda_o(295)$ Using the Matyushov Model for $\Delta_r G(T)$

	method 2[a]		method 3[b]	
solvent	$\lvert V\rvert$, cm^{-1}	$\lambda_o(295)$, eV	$\lvert V\rvert$, cm^{-1}	$\lambda_o(295)$, eV
benzene	5.7	0.124	5.1	0.069
toluene	8.8	0.213	5.7	0.132
cumene	6.6	0.181	4.8	0.129
mesitylene	5.6	0.143	4.2	0.094
TIP[c]	0.7	0.002	1.2	0.027

[a] In method 2, $d\lambda_o(T)/dT$ is taken from the Matyushov model. [b] In Method 3, $\lambda_o(T)$ is taken from the Matyushov model. [c] TIP is 1,3,5-triisopropylbenzene.

parameters, such as the solute radius, were chosen to achieve the best global fit (in all solvents). The solid lines in Figure 4 display the resulting fits to the measured reaction free energies. The effective solute sphere radius was set equal to 5.5 Å. The change in the dipole moment between the LE and CT states was set to 34 D. The vacuum free energy change ΔG_{vacuum} was set to 0.568 eV. The LE state polarizability was set to 100 Å^3 and $\Delta\gamma'$ was 2 Å^3. The solvent parameters used are reported in Table 2. The parameter values were obtained in a standard manner[21] for each of the solvents. In each case, the polarizability of the solvent was adjusted (by less than 10%) to improve the fit. The temperature-dependent density, the static dielectric constant and the high-frequency dielectric constant (estimated as n^2) were obtained from the literature.

The parameters determined by fitting $\Delta_r G(T)$ in the various solvents were used to predict the absolute magnitude and the temperature dependence of the reorganization energy $\lambda_o(T)$ in each solvent. The values of $\lambda_o(295)$ predicted by the "calibrated" Matyushov model are all less than 0.15 eV (see Table 4, column 5). In toluene and cumene, the two solvents with nonzero dipole moments, the estimated $\lambda_o(295)$ are moderately larger than in benzene and mesitylene. The λ_{dipole} term, eq 12, is the source of the larger reorganization energy in toluene and cumene (see Appendix B). Before proceeding to the analysis of the kinetic data, it is important to point out that the parameter set used to fit $\Delta_r G(T)$ is not unique. For example, it is possible to decrease the size of the dipole moment change (Δm) and increase the solute polarizability α_0 and still obtain similar quality fits to the data.

(21) Ben-Amotz, D.; Herschbach, D. R. *J. Phys. Chem.* **1990**, *94*, 1038.

V. Determination of $|V|$ and λ_o

Values of $|V|$ and λ_o were extracted from the temperature-dependent rate constant data using three different procedures. First, the rate data was fit using the experimental $\Delta_r G(T)$ and treating λ_o and $|V|$ as temperature independent, but adjustable, parameters. The results of this "*T*-independent" analysis (method 1) are presented in Table 3. This procedure is appropriate for the solvents that exhibit a weak temperature dependence of λ_o when a temperature-independent $|V|$ is assumed; i.e., benzene, toluene, and cumene. This condition is also satisfied in mesitylene at low temperatures, and the data in mesitylene at temperatures below 320 K were analyzed in this manner. Use of this method for the triisopropylbenzene data is reasonable only if $|V|$ is considerably less than 6 cm^{-1}. Given the results of the analysis, an assumption for $|V|$ of 1 cm^{-1} more closely represents the experimental findings (vide infra). In each case the data in Figure 3 was well reproduced by this analysis.

According to Table 3, the best fit parameter values are consistent with an increase in the electronic coupling when the solvent's aromatic ring is able to position between the donor and acceptor π-functions. The benzene and monosubstituted benzene solvents have similar electronic couplings. In contrast, the electronic coupling in mesitylene, which has three bulky methyl groups equally spaced around the periphery of the ring, is ~40% smaller and the coupling in TIP, which has the greatest steric impediment to entry into the cleft, is 4−5 times smaller than that in benzene. The small $|V|$ is consistent with the assumption of a nearly temperature independent λ_o (Figure 6, vide supra). The best fit values of the reorganization energy provide additional insight into the solvent−solute interaction. The reorganization energy in benzene and the monoalkylated benzenes are similar, whereas the reorganization energy in TIP is smaller. The kinetic model does not account for the presence of the cleft in **2**. None the less, the extracted reorganization energies are strongly influenced by the solvent size. From a molecular perspective, reduced entry of the bulky solvents into the solute cleft would be expected to decrease their ability to stabilize the charge-transfer state and to produce smaller values of λ_o.

In a second approach, the electronic coupling was determined by fitting the rate data to eq 6 using the $\Delta_r G(T)$ and $d\lambda_o/dT$ (Table 2) values predicted by the "calibrated" Matyushov model, method 2. In this method, $|V|$ and $\lambda_o(295)$ were the adjustable parameters. The best fit values are reported in Table 4 (columns 2 and 3) and the lines displayed in Figure 3 represent the result of this fitting procedure. This approach does an excellent job of reproducing both the forward and back electron-transfer data in all five solvents. In contrast to method 1, the electronic coupling obtained for the monosubstituted benzenes is larger than benzene. The estimated coupling in mesitylene is comparable to the values found for benzene and the monoalkylated benzenes and the coupling in TIP is more than a factor of 5 smaller than the coupling found in benzene. The room-temperature reorganization energies $\lambda_o(295)$ obtained in this analysis are between 0.22 and 0.12 eV in all solvents except TIP, for which the reorganization energy was found to be < 0.01 eV. The Matyushov treatment predicts that λ_o should be largest in the slightly dipolar solvents cumene and toluene (vide infra). A dissection of the reorganization energy (see Appendix

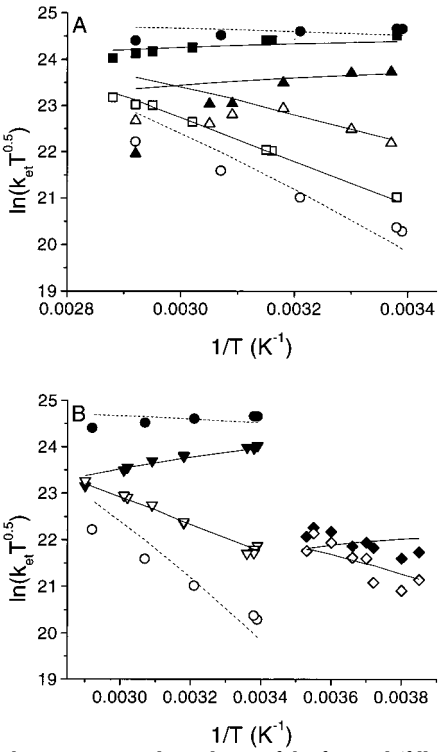

Figure 7. The temperature dependence of the forward (filled symbols) and backward (open symbol) electron-transfer rate constants is shown. Panel A shows the data for benzene (●, ○), toluene (■, □), and mesitylene (▲, △). Panel B shows the data for benzene (●, ○), cumene (▼, ▽), and triisopropylbenzene (♦, ◊). The lines are fits to the data using the Matyushov model for $\Delta_r G(T)$ and $\lambda_o(T)$. The dashed curves show the fits for benzene and the solid curves are for the other solvents.

B) reveals that the dipolar contribution is the source of the larger values in these two solvents. The extracted value of λ_o in TIP is extraordinarily small, but is required to reproduce the observed increase of both the forward and reverse electron-transfer rate constants with increasing temperature.

In a final approach, the electronic coupling was determined by fitting the rate data to eq 6 using the $\Delta_r G(T)$ and $\lambda_o$values predicted by the "calibrated" Matyushov model, method 3. In this method, $|V|$ was the only adjustable parameter. This approach provides a stringent test of the Matyushov model's ability to predict the solvent reorganization energy in aromatic solvents. The best fit values of $|V|$ are reported in Table 4 (column 4) along with the Matyushov model's predictions of $\lambda_o(295)$ (column 5). With the exception of TIP, the $|V|$ generated by method 3 is as much as 40% smaller than that produced by method 2. Likewise, the $\lambda_o(295)$ value from method 3 is ~0.06 eV smaller than that from method 2. For TIP, both $|V|$ and λ_o produced by method 3 are larger. However, as seen in Figure 7, method 3 accurately reproduces the kinetic data in toluene, cumene, and mesitylene but fails to reproduce the proper slope of the Arrhenius plots in benzene and TIP. The origin of this failure can be understood by analyzing the temperature dependence of eq 6 for the $n = 0$ term.[22] Figure 8 displays the dependence of the slope of k_{for} on the value of $\lambda_o(295)$. For TIP, the observed negative slope (•−•) is reproduced only by values of $\lambda_o(295)$ less than 0.01 eV,[23] whereas the Matyushov value of 0.023 eV produces a weak positive slope, as seen in Figure 7. The positive slope of the benzene data (◊−◊) is reproduced by $\lambda_o(295)$ values greater than 0.1 eV, whereas the Matyushov prediction of 0.048 eV results in a negative slope.

(22) In these systems, the $n = 0$ terms contribute greater than 95% of the rate calculated using eq 6.

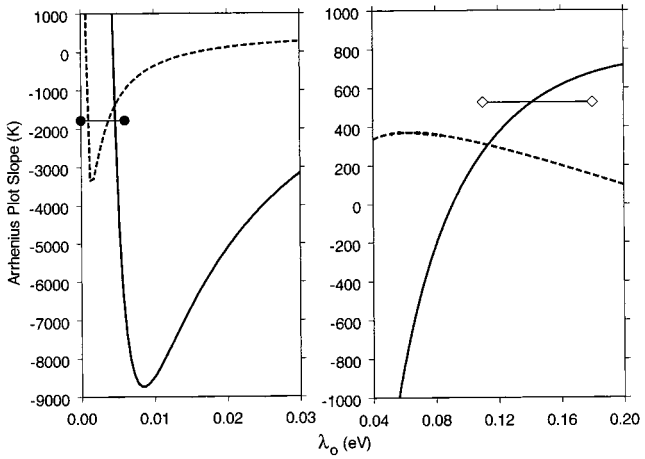

Figure 8. The calculated slope of $\ln(k_{for}(T)\sqrt{T})$ versus $1/T$ is plotted as a function of λ_o for benzene and TIP. The solid curve is for benzene, and the dashed curve is for TIP. The left panel shows the result for 0−0.03 eV. The horizontal line with circles indicates the experimental slope for TIP. The right panel shows the result for 0.04−0.2 eV. The horizontal line with diamonds indicates the experimental slope for benzene.[27]

Plots analogous to Figure 8 for toluene, cumene, and mesitylene predict positive Arrhenius slopes for $\lambda_o(295)$ greater than 0.08 eV. As a result, the fits to the kinetic data and the extracted values of $|V|$ are only moderately affected by the value of $\lambda_o(295)$ in the latter three solvents.

VI. Discussion and Conclusion

The fluorescence decay of **2** in nonpolar and weakly polar solvents is biexponential. The fast component of the decay involves depopulation of the LE state primarily through establishment of an LE ⇄ CT excited-state equilibrium. The slow component arises from irreversible depopulation of the equilibrium mixture to lower energy states.[24] Analysis of the biexponential decay law, in conjunction with the intrinsic decay rate constant for the LE state in donor only analogues, enabled reliable determination of three important quantities: the forward electron-transfer rate k_{for} (LE to CT), the backward electron-transfer rate k_{back} (CT to LE), and the charge separation free-energy $\Delta_r G$. The data in Figure 4 show that the reaction free-energy $\Delta_r G(T)$ becomes increasingly endoergic with increasing temperature and with increasing alkyl substitution of the solvents' aromatic core. The destabilization of the charge-transfer state with temperature may be understood in terms of decreasing solvent density. A molecular model for the solvent is able to mimic the observed temperature dependence in this series of related solvents.

Among the set of solvents investigated, only toluene and cumene possess permanent dipole moments. The latter are small (<0.35 D) and, in fact, benzene appears to be more effective at stabilizing the CT state. Benzene's axial quadrupole moment is slightly larger than toluene's[13a] and, at least from one edge, the unsubstituted benzene ring can get closer to the solute CT state. Although quadrupole contributions to solvation could be significant, the molecular model used here does not include them. The model incorporates the steric/size factor through the

(23) The λ_o value less than 0.003 eV also produces the experimental slope at the indicated temperature; however, use of this λ_o leads to a 5 order of magnitude reduction in the rate constant over the experimental temperature range, in contrast to the small change that is observed.

(24) In benzene, greater than 20% of the CT state of **2** decays by intersystem crossing to form the anthracene triplet state. Professor J. Goodman (University of Rochester), unpublished results.

solvent's effective hard-sphere diameter, as indicated in Table 2. Although the molecular polarizability is larger in the more highly alkylated solvents, their size is also larger, and the $\rho\alpha$ contribution to the dipolar density remains relatively constant in these solvents. It appears that the differences in the solvation can be attributed to the smaller effective diameter of the less alkylated solvents and changes in the packing fraction η (see Table 2 and Appendix B).

The same model and parameters that adequately reproduced $\Delta_r G(T)$ in the different solvents was used to predict the magnitude and temperature dependence of the outer-sphere reorganization energy. The parametrized Matyushov model prediction of the $\lambda_o(295)$ values are all less than 0.15 eV (Table 4). For the three nondipolar solvents, increased solvent size (sphere diameter), molecular polarizability, and Lennard-Jones energy reduce the reorganization energy from 0.069 eV in benzene to 0.039 eV in mesitylene and to 0.027 eV in TIP. For the nondipolar solvents, λ_{dipole} makes no contribution to the overall reorganization energy. However, the presence of a small dipole moment in toluene and cumene increases the overall reorganization energy 2-fold in comparison to, the otherwise similar solvent, benzene. As the dipole moment of cumene is 25% larger than that of toluene, one expects the predicted $\lambda_o(295)$ value to be greater for cumene. However, the increased size of cumene reduces the induction contribution $\lambda_{induction}$ which offsets the increased dipolar contribution λ_{dipole} (Appendix B). As a result, the predicted reorganization energies $\lambda_o(295)$ in these two solvents are quite similar.

The molecular model predicts a weak decrease of λ_o with increasing temperature (Table 2) which is corroborated by optical studies of CT emission and absorption bands in benzene[25] and other weakly polar solvents.[26] The "parametrized" Matyushov model predicts $d\lambda_o/dT$ values (Table 2) of about -7×10^{-4} eV/K in the dipolar solvents toluene and cumene and of -1×10^{-4} eV/K in TIP. From a practical standpoint, the parametrized Matyushov model does a reasonable job considering that it does not account for the detailed shape of the molecule. It predicts λ_o values that are remarkably close to those required by the observed k_{ET} temperature dependence (Figure 8) and from a best fit to the data.

With the parametrization of a reasonable model for the temperature dependence of the reaction free energy and the outer-sphere reorganization energy, it was possible to fit the temperature-dependent electron-transfer rate constants to the semiclassical model (eq 6) and determine $|V|$. The results from the three analyses of the kinetic data clearly demonstrate that $|V|$ is smaller in an aromatic solvent that is too bulky to effect simultaneous overlap with the π-functions of the donor and acceptor groups. The analyses for the benzene, toluene, and cumene solvents give electronic couplings that are similar ($\sim$6 cm^{-1}). For 1,3,5-triisopropylbenzene, $|V|$ is at least five times smaller than in benzene. The possibility that a smaller value of $|V|$ is obtained as a result of the parametric dependence on the value of λ_o in eq 6 has been evaluated. Figure 5 demonstrates that even if an identical value of λ_o is assumed for this series of solvents, the calculated electronic coupling is at least 3-fold smaller for TIP than for benzene. These experiments emphasize once again the difficulty in interpreting electron-transfer rate constants determined at a single temperature. Without independent characterization of λ_o and $\Delta_r G$, a single rate measurement can be interpreted to support any number of conclusions.

The variation of $|V|$ with solvent may be rationalized in terms of the effect of the alkyl group steric bulk on the solvent's tendency to enter the cleft of **2** and on the resulting interactions with the D and A groups. For benzene and monosubstituted benzenes, the aromatic core can enter the cleft of **2** with minimal conformational restrictions. The comparable couplings determined for benzene, toluene and cumene suggest similar geometries and probabilities of solvent insertion into the cleft of **2** for all three solvents. For 1,3,5-triisopropylbenzene, the bulky isopropyl groups inhibit entry of the aromatic core into the cleft of **2**, causing a decrease in the electronic coupling by increasing the solvent-to-donor and solvent-to-acceptor distance. It is possible for an isopropyl group on TIP to insert into the cleft, thus providing a solvent-mediated path for D−A coupling, albeit a less effective one. Mesitylene affords an intermediate value of the coupling. The methyl groups are slightly wider than the aromatic ring. Their presence may decrease the overlap of the ring orbitals with the donor and acceptor groups when mesitylene is located in the cleft. Alternatively, they may limit the available conformations that lead to significant electronic coupling or decrease the time average probability of finding solvent in the cleft. Further studies are required to distinguish these possibilities. The key may lie with the unusual kinetic behavior at higher temperatures in mesitylene.

We have shown that a prerequisite for effective aromatic solvent mediation of electronic coupling is placement of the aromatic core directly between the donor and acceptor groups. One way to hinder a solvent's access into the cleft is to increase its steric bulk. The results of this investigation demonstrate that preventing solvent entry into the cleft significantly reduces the efficacy of solvent-mediated coupling in electron-transfer reactions.

Acknowledgment. This work was supported in part by the National Science Foundation (Grants CHE-9708351 (M.B.Z.) and CHE-941693 (D.H.W.)). D.H.W. was the Belkin Visiting Professor at the Weizmann Institute of Science during part of this work. We gratefully acknowledge numerous helpful discussions with Dr. Dmitry Matyushov (University of Utah).

Note Added in Proof

Recently Matyushov and Voth [*J. Chem. Phys.* **1999**, *111*, 3630] published an extension of the Matyushov model to include quadrupolar interactions. Application of this model to the data does not change the conclusions, as will be discussed in a forthcoming work.

Appendix A

The dipolar solvent response contains contributions from both solute−solvent and solvent−solvent interactions. Matyushov has shown that

$$P(y,\rho^*,r_o) = \frac{yI_{0s}^{(2)}}{1 + yI_{0s}^{(3)}/I_{0s}^{(2)}}$$

where $I^{(2)}$ and $I^{(3)}$ are the two and three particle solute−solvent integrals approximated by

(25) Vath, P. A.; Zimmt, M. B. Unpublished results.

(26) (a) Tepper, R. J.; Zimmt, M. B. *Chem. Phys. Lett.* **1995**, *241*, 566. (b) Cortés, J.; Heitele, H.; Jortner, J. *J. Phys. Chem.* **1994**, *98*, 2527.

(27) The calculation of these curves requires values of $\Delta_r G(T)$, $d\Delta_r G(T)/dT$ and $d\lambda_o(T)/dT$. The $\Delta_r G(T)$ and $d\Delta_r G(T)/dT$ were obtained from the experimental data. The $d\lambda_o(T)/dT$ was evaluated by the Matyushov model.

$$\text{slope} = \left[-\frac{(\Delta G + \lambda)^2}{4\lambda k_B}\right] + \frac{(\Delta G + \lambda)T}{2\lambda k_B}\left(\frac{\partial(\Delta G)}{\partial T}\right) + \frac{T}{k_B}\left[\frac{2\lambda k_B T + 2\lambda(\Delta G + \lambda) - (\Delta G + \lambda)^2}{4\lambda^2}\right]\left(\frac{\partial \lambda}{\partial T}\right)$$

$$I_{0s}^{(2)} = \frac{1}{r_o^3} + \frac{d(\rho^*)}{r_o^4} + \frac{e(\rho^*)}{r_o^5} + \frac{f(\rho^*)}{r_o^6}$$

$$I_{0s}^{(3)} = \frac{a(\rho^*)}{r_o^3} + \frac{b(\rho^*)}{r_o^4} + \frac{c(\rho^*)}{r_o^5}$$

$$I_{0s}^{(4)} = \frac{1}{r_o^9} + \frac{a(\rho^*)}{r_o^{10}} + \frac{b(\rho^*)}{r_o^{11}} + \frac{c(\rho^*)}{r_o^{12}}$$

The coefficients $a(\rho^*)$, $b(\rho^*)$, $c(\rho^*)$, etc. in the density expansion have been fitted to the calculated dependencies of the solute−solvent integrals and are provided in ref 8a. The explicit form of these integrals is given in ref 8c.

The integrals found in eqs 11, 14, and 15 were evaluated using the Pade form for the integrals. In our calculations,

$$\int_{\sigma_{ij}^{0s}}^{\infty} u_1^{0s}(r) g_{0s}^{(0)}(r) r^2 \, dr = \left[\frac{I_{0s}^{(4)}}{9} - \frac{I_{0s}^{(2)}}{3}\right]$$

$$9\int_{r_0}^{\infty} \frac{g_{0s}^{(0)}(r)}{r^{10}} dr = I_{0s}^{(4)}$$

$$\left[\int_0^{\infty} u_1^{0s}(r)^2 g_{0s}^{(0)}(r) r^2 \, dr - (1 - m_{ss}(0)) \int_0^{\infty} u_1^{0s}(r) u_1^{0s}(r+\phi) g_{0s}^{(0)}(r) g_{0s}^{(0)}(r+\phi) r(r+\phi) \, dr\right] = I_{0s}^{(4)}$$

The latter integral ignores the contribution from three-body interactions. An effect which becomes increasingly important as the polarity of the solvent increases.

Table 5

T, K	ΔG_{dipole}, eV	$\Delta G_{dispersion}$, eV	ΔG_{total}, eV	λ_{dipole}, eV	$\lambda_{dispersion}$, eV	$\lambda_{induction}$, eV	λ_{total}, eV
			benzene				
296	−0.667	−0.018	−0.116	0	0	0.069	0.069
312	−0.648	−0.017	−0.096	0	0	0.065	0.065
326	−0.632	−0.017	−0.080	0	0	0.062	0.062
342	−0.613	−0.016	−0.061	0	0	0.058	0.058
			toluene				
296	−0.631	−0.025	−0.087	0.038	0	0.094	0.132
316	−0.608	−0.024	−0.063	0.034	0	0.083	0.118
331	−0.591	−0.024	−0.046	0.032	0	0.076	0.108
339	−0.582	−0.023	−0.037	0.031	0	0.072	0.104
347	−0.573	−0.023	−0.028	0.030	0	0.069	0.099
			mesitylene				
297	−0.552	−0.050	−0.033	0	0.001	0.092	0.093
303	−0.547	−0.049	−0.027	0	0.001	0.089	0.090
314	−0.537	−0.048	−0.016	0	0.001	0.084	0.085
324	−0.528	−0.048	−0.007	0	0.001	0.080	0.081
342	−0.512	−0.046	0.011	0	0.001	0.073	0.074
			cumene				
296	−0.591	−0.032	−0.054	0.042	0.001	0.086	0.129
314	−0.573	−0.031	−0.036	0.039	0.001	0.076	0.115
324	−0.563	−0.031	−0.025	0.037	0.001	0.070	0.108
331	−0.556	−0.031	−0.018	0.036	0.001	0.067	0.103
345	−0.543	−0.031	−0.005	0.033	0	0.060	0.094
			TIP				
260	−0.540	−0.047	−0.018	0	0.001	0.029	0.030
263	−0.538	−0.046	−0.016	0	0.001	0.029	0.030
278	−0.527	−0.046	−0.003	0	0.001	0.027	0.028
282	−0.524	−0.045	0	0	0.001	0.027	0.028

Appendix B

Table 5 shows the different contributions to ΔG and λ from the dipolar, induction and dispersion interactions, according to the Matyushov model.

JA992281K